

Graph Attention Networks for Channel Estimation in RIS-assisted Satellite IoT Communications

Kürşat Tekbıyık, *Graduate Student Member, IEEE*, Güneş Karabulut Kurt, *Senior Member, IEEE*,
Ali Rıza Ekti, *Senior Member, IEEE*, Halim Yanikomeroglu, *Fellow, IEEE*

Abstract—Direct-to-satellite (DtS) communication has gained importance recently to support globally connected Internet of things (IoT) networks. However, relatively long distances of densely deployed satellite networks around the Earth cause a high path loss. In addition, since high complexity operations such as beamforming, tracking and equalization have to be performed in IoT devices partially, both the hardware complexity and the need for high-capacity batteries of IoT devices increase. The reconfigurable intelligent surfaces (RISs) have the potential to increase the energy-efficiency and to perform complex signal processing over the transmission environment instead of IoT devices. But, RISs need the information of the cascaded channel in order to change the phase of the incident signal. This study evaluates the pilot signal as a graph and incorporates this information into the graph attention networks (GATs) to track the phase relation through pilot signaling. The proposed GAT-based channel estimation method examines the performance of the DtS IoT networks for different RIS configurations to solve the challenging channel estimation problem. It is shown that the proposed GAT both demonstrates a higher performance with increased robustness under changing conditions and has lower computational complexity compared to conventional deep learning methods. Moreover, bit error rate performance is investigated for RIS designs with discrete and non-uniform phase shifts under channel estimation based on the proposed method. One of the findings in this study is that the channel models of the operating environment and the performance of the channel estimation method must be considered during RIS design to exploit performance improvement as far as possible.

Index Terms—IoT networks, LEO satellites, non-ideal reconfigurable intelligent surfaces, graph attention networks.

I. INTRODUCTION

Internet of things (IoT) networks are expected to grow with approximately 20% in terms of compound annual growth [1]. In other words, more than 100 billion devices will be connected in massive ubiquitous networks [2, 3]. This growth brings a backhauling gap for the omnipresently connected

massive number of IoT devices. In this context, dense low-Earth orbit (LEO) satellite deployments can be an enabler for global service of IoT devices. Low-power LEO satellites have been already in service [4]. However, a new paradigm, which is called direct-to-satellite (DtS), has recently emerged to connect IoT devices directly to satellites without any gateways on the ground [5].

Even though geostationary orbit (GEO) satellites have been proposed for narrowband-IoT applications [6, 7], high delay and high path loss caused by the distance between GEO satellites and the Earth reduce the energy-efficiency. On the other hand, LEO satellite constellations become a prominent way to support global IoT network with a reasonable path delays [8, 9]. Furthermore, the required transmit power for LEO orbits is lower due to the relatively short distance to Earth. For LEO satellite assisted IoT communications, two methods are employed: indirect link and direct (i.e., DtS) transmission links. Direct access is preferred due to the following reasons: the cost of the gateway infrastructure, temporary device deployments for specific environments, and operation ability after any disaster [4]. However, DtS requires a steerable antenna at ground stations (i.e., IoT devices) for tracking owing to the motion of LEO satellites. Furthermore, a sophisticated transceiver is needed in IoT devices to recover the received signal. Considering the hardware limitation and battery capacity for IoT devices, these requirements cannot be met. Rather than an advanced transceiver in each IoT device, it is possible to apply complex signal processing methods over the propagation medium [10].

Smart artificial surfaces, referred to as reconfigurable intelligent surface (RIS), have been recently proposed to shift the processes on the receiver to the propagation medium by adjusting the incident wave phase [11]. In other words, coding or complex processing is not needed by RISs. The most appealing feature of RISs is to comprise only passive elements with a single RF chain [12]. It is worth noting here that saturation on RISs is not expected due to the all-passive element structure of RISs although the distance between transmitter and RIS is close. Thus, the use of RIS fits well with LEO satellites considering their size, weight, and power (SWaP) constraints [13]. The recent prototypes [14–16] demonstrate that it is possible to decrease the size and weight of the transceiver compared to the conventional multiple-input multiple-output (MIMO) systems. Moreover, the battery life of IoT devices is extended because of decreasing processing energy [17]. It should be highlighted that RISs can be a game-changer for DtS IoT systems since RISs can reduce

K. Tekbıyık is with the Department of Electronics and Communications Engineering, İstanbul Technical University, İstanbul, Turkey, e-mail: tekbiyik@itu.edu.tr

G. Karabulut Kurt is with the Poly-Grames Research Center, Department of Electrical Engineering, Polytechnique Montréal, Montréal, Canada, e-mail: guenes.kurt@polymtl.ca

A.R. Ekti is with the Grid Communications and Security Group, Electrification and Energy Infrastructure Division, Oak Ridge National Laboratory, Oak Ridge, TN, U.S.A., e-mail: ektia@ornl.gov. This manuscript has been authored in part by UT-Battelle, LLC, under contract DE-AC05-00OR22725 with the US Department of Energy (DOE). The publisher acknowledges the US government license to provide public access under the DOE Public Access Plan (<http://energy.gov/downloads/doe-public-access-plan>).

H. Yanikomeroglu is with the Department of Systems and Computer Engineering, Carleton University, Ottawa, Canada, e-mail: halim@sce.carleton.ca

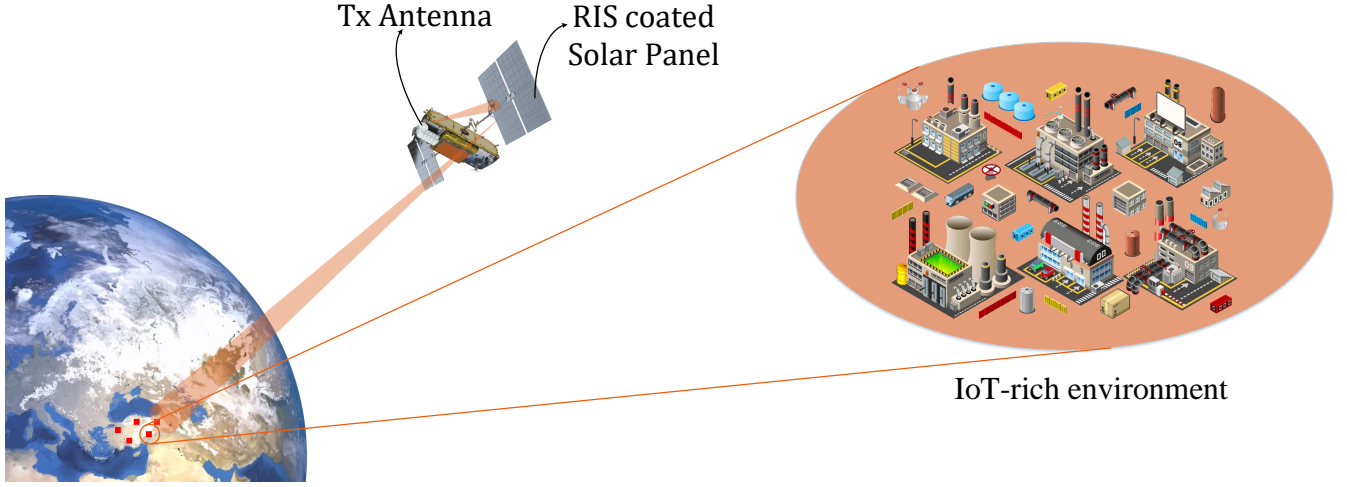


Fig. 1. It is possible to enhance the QoS for satellite-IoT systems by utilizing RIS. Therefore, the required power can be reduced for the same data rate and error probability.

both the required transmit power and hardware complexity. Furthermore, our previous works [13, 18] present that RISs can improve the system performance for LEO inter-satellite links and achievable data rate for satellite-IoT systems, respectively. It is demonstrated that utilizing RISs in DtS system provides two-fold advantages. By focusing the beam towards the receiver, signal-to-noise ratio (SNR) can be maximized while maintaining the same transmit power. The second advantage is the decrease in computational complexity of the transceiver by processing the transmitted signal on the propagation medium rather than on the receiver.

The current literature clearly shows that RISs can provide many attractive features for DtS IoT systems. A few of these are the energy-efficiency, improved achievable rate, beamforming, and tracking. However, in order to take advantage of all these attractive features, channel state information (CSI) must be obtained properly. The main challenge in channel estimation for RIS-assisted communications is that the received signal includes cascaded channel coefficients. To cope up with the channel estimation problem, some methods have been proposed. The first methodology [19, 20] utilizes a conventional view for channel estimation by activating a single RIS element for each time instance during the training phase. In other words, the channel coefficients are individually estimated by switching RIS elements on and off. Considering the switching time and total pilot overhead, it can be concluded that this method cannot be efficiently employed on RIS-assisted DtS system because of the longer training signal than channel coherence time [21]. Concisely, acquired channel coefficients regarding RIS elements by this method are not time-invariant. In [22], the compressive sensing is employed to decrease pilot training overhead. But, its iterative approach to solving a non-convex problem might require longer computation time for simple-hardware systems. It is known that RISs comprise only passive reflecting/scattering elements; hence, they cannot acquire CSI by themselves. A recent approach in [23] designs RIS in which some elements are active to estimate channel coefficients at RISs. Please note that increasing the number of

active elements on RIS means that problems related to SWaP constraints will probably arise. Therefore, this method is not desired for satellite systems.

To address the challenges related to the channel estimation in RIS-assisted wireless communications, we have recently proposed a channel estimator based on graph attention network (GAT) [24]. It should be noted that to the best knowledge of the authors, there is no channel estimation method based on graph neural networks except our recent work on the GAT channel estimator, yet. The motivation behind using GATs for channel estimation can be listed as (i) GATs can estimate all channel coefficients without an on-off switch mechanism, (ii) GATs' computational complexity is relatively low [25], (iii) GATs can be generalized over unobserved graphs due to the attention mechanism [26]. Briefly, the GAT channel estimator can reduce lower pilot overhead as it requires a single pilot signaling subframe to estimate channel coefficients regarding all RIS elements. Furthermore, GAT estimator can continue to perform well under variable channel conditions, thanks to the attention mechanism [24].

Moreover, this study investigates bit error rate (BER) performance of the DtS systems under more practical RIS designs unlike the prior works [13, 27, 28] on wireless communications assisted by hypothetical RISs with continuous phase shift capability. While hypothetical RISs show almost independent performance from the channel model, the performance of practical RISs is significantly dependent on both the characteristics of the channel they operate and the performance of the channel estimation method, depending on their design. Therefore, the channel model and the channel estimation algorithm should be considered together when investigating the performance of practical RISs.

It has been shown in our previous work [18] that it is possible to increase energy-efficiency by using RISs. However, as RISs strictly need CSI to improve the received SNR, we propose a channel estimation architecture based on GATs in [24] which overperforms least square (LS) estimation. Although [24] made significant contributions as a proof-of-

concept study, it was lacking in many aspects. This study is significantly extending the work in this field by presenting the following main contributions:

- C1 By comparing the channel estimation performance of the proposed GAT model and the conventional deep learning (DL) methods, it is shown that the GAT shows a higher performance at low SNR. Moreover, the GAT can maintain its performance much more than the conventional DL methods under unobserved channel conditions. It should be noted that the proposed GAT is less time-consuming for training due to its short epoch time compared to the conventional DL methods.
- C2 In addition to channel estimation, we design time-division duplex (TDD) framework for uplink and downlink signaling of RIS-assisted DtS IoT in order to use partial channel reciprocity. Due to the motion of satellites, the coherence time is short. Thus, the pilot signaling subframe must be extremely short duration while the channel estimation method should show high performance with the small number of pilot symbols. In this study, the proposed GAT estimator uses only 16 symbols for the pilot subframe.
- C3 The performance of RIS-assisted DtS IoT is investigated for non-ideal RISs with discrete and distinct phase sets as well as ideal RISs when CSI is acquired by the proposed GAT channel estimator. By considering the numerical results, the relation between RIS design and the channel models is discussed.

The rest of this paper is organized as follows. Section II introduces the basic background for GATs and RIS-assisted satellite communications. In Section III, the system model is detailed for RIS-assisted DtS IoT supported by GAT channel estimator. Section IV describes the channel estimation procedure from dataset generation to training by giving the related parameters for GAT. In Section V, numerical results under various RIS configurations are discussed. Finally, Section VI dwells on the open issues and concludes the study.

II. PRELIMINARIES

In this section, the fundamentals for each part of the proposed RIS-assisted satellite IoT communication with GATs channel estimator are introduced. First, we present the GAT in detail. Then, RIS-assisted satellite links are discussed. It should be noted that the notation used in this section is given for downlink; however, it can be used for uplink transmission without loss of generality.

A. Graph Attention Networks

Graph neural networks have been recently proposed as a state-of-the-art solution for data that does not exhibit a grid-like structure while most deep learning methods are utilized for the data in the regular domain. GAT, which is one of the graph neural networks, is prominent for inductive learning thanks to its attention mechanism. Inductive learning provides the generalization of a trained network over unobserved graphs. Considering the random nature of the propagation medium, GAT is suitable to be utilized over unobserved channel states.

A GAT consists of graph attention layers (GALs) with P input nodes denoted by $\vartheta = \{\vec{\vartheta}_1, \vec{\vartheta}_2, \dots, \vec{\vartheta}_P\}$, $\vec{\vartheta}_i \in \mathbb{R}^F$. F stands for the number of features in each node. The output set of node features for GAL can be shown by a new set $\vartheta' = \{\vec{\vartheta}'_1, \vec{\vartheta}'_2, \dots, \vec{\vartheta}'_P\}$, $\vec{\vartheta}'_i \in \mathbb{R}^{F'}$. Since the cardinality for the output and input might be different, the number of features is represented by F' . The input properties of each node are transformed to higher-level properties by utilizing a linear transformation described by the weight matrix, $\mathbf{W} \in \mathbb{R}^{F \times F'}$. Then, the attention mechanism, $a : \mathbb{R}^{F'} \times \mathbb{R}^{F'} \rightarrow \mathbb{R}$, is employed to evoke the self-attention on nodes. The attention coefficients are computed as follows:

$$c_{ij} = a(\mathbf{W}\vec{\vartheta}_i, \mathbf{W}\vec{\vartheta}_j), \quad (1)$$

where c_{ij} denotes the neighborhood between the i -th and j -th nodes in the graph. The attention coefficients reveal how much the features of the j -th node have an impact on the i -th node. By using a softmax function, the attention coefficients are normalized as given [29]

$$\alpha_{ij} = \text{softmax}_j(c_{ij}) = \frac{\exp(c_{ij})}{\sum_{k \in \mathcal{N}_i} \exp(c_{ik})}, \quad (2)$$

where the neighborhood for i -th node is denoted by \mathcal{N}_i . The attention mechanism determines the normalized coefficients, α_{ij} , as [25]

$$\alpha_{ij} = \frac{\exp(\text{ReLU}(\mathbf{a}^\top [(\mathbf{X}\mathbf{W})_i \| (\mathbf{X}\mathbf{W})_j]))}{\sum_{k \in \mathcal{N}(i)} \exp(\text{ReLU}(\mathbf{a}^\top [(\mathbf{X}\mathbf{W})_i \| (\mathbf{X}\mathbf{W})_k]))}, \quad (3)$$

where $\mathbf{X} \in \mathbb{R}^{P \times F}$ and $\mathbf{a} \in \mathbb{R}^{2F'}$ are node features and attention kernel, respectively. The convolution operation is performed over the graph network as follows:

$$\mathbf{Z} = \alpha \mathbf{X} \mathbf{W} + \mathbf{b}, \quad (4)$$

where \mathbf{b} refers to the trainable bias vector. The inputs of this layer are the node attributes matrix $\mathbf{X} \in \mathbb{R}^{P \times F}$, the edge attributes matrix $\mathbf{E} \in \mathbb{R}^{P \times P \times S}$, and the binary adjacency matrix $\mathbf{A} \in \{0, 1\}^{P \times P}$. Moreover, a pooling layer is employed to generalize graph convolution networks [26]. Besides generalization, the pooling layer enables to decrease in the number of representations. As a result, it can be said that the pooling layer avoids the graph neural network to overfit. We employ only a global attention pooling layer in the proposed graph neural network. The output of global attention pooling for the input, \mathbf{X} , can be given as

$$\mathbf{X}' = \sum_{i=1}^P (\sigma(\mathbf{X}\mathbf{W}_1 + \mathbf{b}_1) \odot (\mathbf{X}\mathbf{W}_2 + \mathbf{b}_2))_i. \quad (5)$$

In (5), σ denotes the sigmoid function and \odot is the broadcast elementwise product.

B. RIS-assisted LEO Satellite Communications

In this section, we introduce a system model of RIS-assisted DtS communications for IoT networks. As known that relays can show higher performance when they become closer to the receiver or the transmitter, RIS is deployed near the satellite

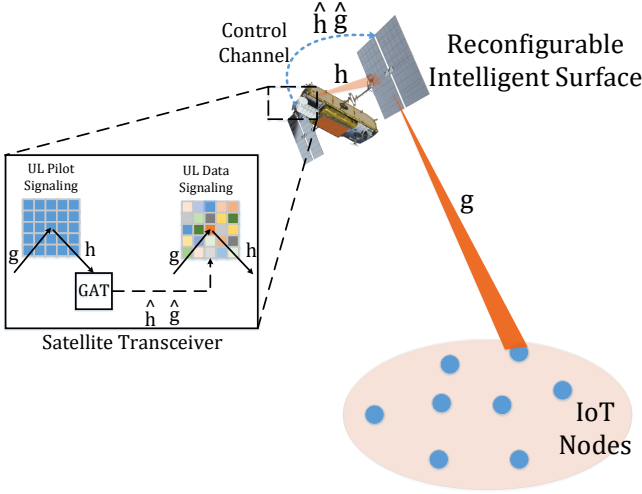


Fig. 2. Direct-to-Satellite IoT communications assisted by RIS with the GAT channel estimator. The estimated channel state information is employed to reconfigure RIS elements.

antenna as illustrated in Fig. 2. Thus, the system scheme provides a two-fold gain which is maximizing improvement and avoiding extra wireless fronthaul between transmitter and RIS for CSI. It is worth noting that it is assumed that the satellite antenna is aligned with the normal line of the RIS to maximize the normalized radiation pattern [18] and the transmit antenna is in the far-field of the RIS to enable beamforming [30]. Under this system model, the received signal reflected by RIS, r , can be given as

$$r = \sqrt{P_t \xi} \mathbf{g}^T \mathbf{\Phi} \mathbf{h} x + w, \quad (6)$$

where the transmitted signal with power P_t and additive white Gaussian noise (AWGN) at receiver are shown by x and $w \sim \mathcal{CN}(0, N_0)$, respectively. ξ is the total path loss in RIS-assisted communications, as detailed in [18]. As the transmit antenna is near the RIS, it is worthwhile to employ the near-field beamforming scheme against the attenuation due to atmosphere [18]. $\mathbf{h} = [h_1, h_2, \dots, h_N]$ and $\mathbf{g} = [g_1, g_2, \dots, g_N]$ stand for the channel coefficient vectors, where $h_i = \beta_i e^{j\theta_i}$ and $g_i = \rho_i e^{j\psi_i}$. In this study, the amplitude coefficients, β_i and ρ_i , are assumed to follow the Rician distribution with the shape parameter of $K = 10$ to evaluate a slight multipath fading [31–33]. θ_i and ψ_i denote the phase response of the channels regarding the i -th RIS element. Also, $\mathbf{\Phi}$ is the RIS phase shift matrix given as

$$\mathbf{\Phi} = \text{diag} \{ A_1 e^{-j\phi_1}, \dots, A_N e^{-j\phi_N} \}, \quad (7)$$

where ϕ_i and A_i denote the phase and amplitude response of i -th RIS element, respectively. It is worth mentioning that RIS is assumed as a lossless device throughout this study; hence, $A_i = A = 1$, $\forall i$. Besides, ϕ_i is determined through the estimated channel coefficients, \hat{h}_i and \hat{g}_i , as follows:

$$\phi_i = \hat{\theta}_i + \hat{\psi}_i, \quad (8)$$

where $\hat{\theta}_i$ and $\hat{\psi}_i$ are the phase shift values estimated by the GAT channel estimator.

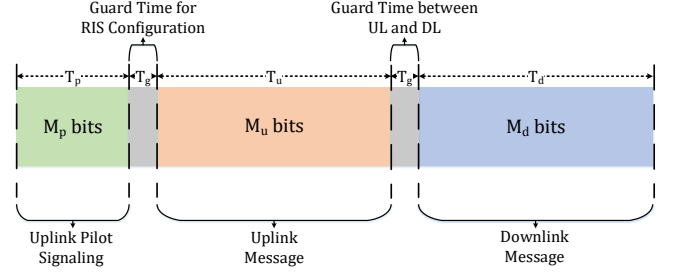


Fig. 3. Each TDD frame consists of uplink pilot signaling, uplink message and downlink message subframes. The frame starts with pilot signaling to estimate channel coefficients regarding to RIS elements.

Then, the instantaneous effective SNR, γ^{eff} , is given as follows:

$$\gamma^{\text{eff}} = \frac{P_t \xi \left| \left(\sum_{i=1}^N \beta_i \rho_i e^{j\psi_i} \right) \right|^2}{N_0}, \quad (9)$$

where $\psi_i = \phi_i - \theta_i - \nu_i$ and $\psi_i = 0$ for the ideal channel estimation.

III. DIRECT-TO-SATELLITE IoT COMMUNICATIONS

In this section, LEO satellite-enabled IoT communications system model is introduced. Before detailing the system model, we would describe the motivations behind the proposed system model. In this study, a narrowband modulation-based physical layer is adopted. This scheme utilizes a signal with a carrier which has very narrow bandwidth. By employing this scheme, it is possible to design low-complex transceivers [34]. Thus, the cost for the transceiver part of IoT devices can be reduced. Moreover, it should be noted that narrow band modulation can show resistance to noise and interference due to its high power spectral density [35]. Therefore, it is possible to employ ultra-narrow band signals on shared frequency bands. Another appealing feature of ultra-narrow band modulation is that it enables long-range communication link with low-power consumption [36]. As a result, ultra-narrow band modulation techniques can provide to employ low-complex transceiver design in both satellite and IoT devices. Moreover, it can increase battery life by using low power for transmission and reception. However, besides all the appealing features of ultra-narrow band, data rates supported by the ultra-narrow band signals are very low.

Two methods can be proposed to increase the data rate: increasing the modulation degree and/or increasing the bandwidth. Since the required received SNR value raises with increasing the modulation degree, the transmission power should also be enhanced. This reduces energy-efficiency. Since increasing the bandwidth increases the in-band noise in the receiver, it is evident to increase the transmitted power. More importantly, the equalizer is required in the receiver in order to mitigate multipath fading. To improve energy-efficiency, we have recently proposed RIS-assisted satellite IoT communications in [18]. In this study, we revise the link budget analysis and achievable capacity for RIS-assisted satellite IoT communication under the assumption of the

perfect channel state information. [18] shows that RISs can achieve significant improvement in energy-efficiency for both uplink and downlink. Due to improved energy-efficiency, the transmit power is relatively low in both links. Furthermore, the hardware complexity of IoT devices might decrease because of no shortage of complex amplifiers. Although it might be thought that there is no need for an equalizer in narrowband communication, equalization is required for finding channel gain to compensate for channel effect, and then demodulate the received signals. Several studies such as [37–41] have already addressed the channel equalization for narrow band communication schemes. However, the computational complexity of the proposed methods is high and they either need high computational capacity or consume high power. Noting that RISs are devices that can process signals at rather than transmitter and receiver, the transceiver complexity can be reduced. Moreover, RISs can perform equalizer tasks over a communication medium instead of transceivers [10, 42].

We adopt TDD for uplink and downlink communications to exploit partial channel reciprocity. By uplink pilot signaling, the CSI is estimated in the satellite by utilizing GATs as detailed in Section IV. Each TDD frame includes M_p uplink pilot symbols, M_u uplink message symbols, and M_d downlink message symbols. Furthermore, the TDD frame consists of guard intervals for RIS configuration and avoids interference between uplink and downlink signals. The TDD frame is illustrated in Fig. 3. It is worth noting that the total length of TDD subframe is less than the coherence interval. The M_p -length pilot symbols are selected as a pseudo-noise (PN) sequence generated by the polynomial given by $x^4 + x^2 + 1$. Using PN sequence provides time synchronization between satellite and IoT devices and the detection of the starting point of TDD frame. Additionally, PN sequence might be utilized to identify IoT device by assigning unique sequences for each device.

After channel estimation, RIS elements are configured to maximize the received SNR. Then, the uplink signal can be demodulated without a complex equalizer because RIS can mitigate the random behavior of wireless channels. For downlink communication, the configured RIS is illuminated by the transmitter antenna on the satellite. The reflected signal reaches the IoT device with a high SNR. In consequence, IoT device can demodulate the reflected signal with low power consumption [18].

This scheme mandates having an uplink pilot signal for channel estimation before downlink, and therefore sending a message in the downlink depends on the presence of uplink communication. However, when a satellite needs to send a downlink message without waiting for a message from the uplink, the target IoT devices can be evoked by operating RIS in broadcasting mode. Evoked IoT sends uplink pilot sequence for channel estimation.

It is important to note that the proposed scheme is well suited to random time multiple access techniques such as ALOHA and time-slotted ALOHA or time division multiple access (TDMA). However, random frequency multiple access can be supported by providing extra functionalities to the system. For example, a wideband RIS design is required for

TABLE I
SUMMARY OF THE DATASET PARAMETERS EMPLOYED DURING TRAINING AND TEST.

Parameters	Training	Test
PN Polynomial	$x^4 + x^2 + 1$	$x^4 + x^2 + 1$
Modulation	BPSK	BPSK
# of Samples per SNR	1000	500
SNR (dB)	-30:2:0	-30:2:10
K	10	10
M_p	16	16
N	16, 32, 64	16, 32, 64

multiple access based on frequency domain.

IV. CHANNEL ESTIMATION PROCEDURE

This section is devoted to introducing the proposed channel estimation methodology with GATs. As mentioned earlier, the attractive functionality of GATs that allows it to generalize to graphs that have not been completely observed during training [25] makes it a healer for channel estimation in RIS-assisted communications. Unlike the channel estimation methods such as [19, 20] based on switching RIS elements, the proposed GAT channel estimator is able to acquire all channel coefficients regards to RIS elements in a single pilot signaling subframe. Due to the motion of LEO satellites, channel coefficients rapidly change. Therefore, accurate channel estimation in LEO satellites requires a generalizable network to keep estimation performance stable. As mentioned above, it is possible to generalize GATs to unobserved graphs [25].

A. Dataset Generation

The channel coefficients, \mathbf{h} and \mathbf{g} , are estimated at the satellite by using uplink pilot signaling. To do this, M_p -length pilot subframes are created by using PN sequence generated by the polynomial $x^4 + x^2 + 1$. Assigning different PN sequences to each IoT device allows both identifying the device at the satellite side and maintaining synchronization. Since the DtS IoT systems rely on narrowband modulation schemes [4] and the recent studies [7, 43, 44] proposed binary phase-shift keying (BPSK)-based waveforms for both GEO and LEO IoT services, we utilize BPSK for both pilot and message signaling.

All meta-atoms are switched on with zero-phase shift, scilicet unitary phase shift matrix. To include a slight multipath effect in the dataset, we select β_i and ρ_i as Rice distributed with the shape parameter $K = 10$. It is worth noting that the GAT channel estimator can maintain the estimation performance under different multipath characteristics as shown in [24]. By setting the parameters given above, the dataset has been created. The dataset consists of the input regarding the received signal, \mathbf{X} , and the adjacency matrix, \mathbf{A} , for the graph network including the real and imaginary parts of the channel coefficients. \mathbf{X} and \mathbf{A} are expressed as follows:

$$\mathbf{X} = [\text{Re}\{\mathbf{y}\}; \text{Im}\{\mathbf{y}\}] \quad (10)$$

$$\mathbf{A} = \begin{bmatrix} 0 & 1 \\ 1 & 0 \end{bmatrix}. \quad (11)$$

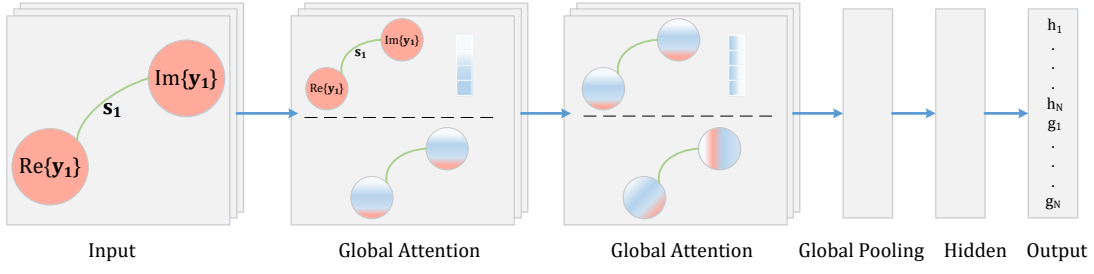


Fig. 4. The illustration for the proposed graph attention network including two consecutive graph attention networks and global attention pooling. The real and imaginary parts of the received signal, \mathbf{y} , are assigned to attributes of two nodes. The edge attributes are set as the pilot symbols, \mathbf{s} .

TABLE II
THE PARAMETERS AND LAYOUT FOR THE PROPOSED GAT CHANNEL ESTIMATOR.

Layers		Dimensions
Inputs	\mathbf{X}	$2 \times M_p$
	\mathbf{A}	2×2
	\mathbf{E}	$2 \times 2 \times M_p$
Labels	\mathbf{y}	$4N \times 1$
Graph Attention 1		2×128
Graph Attention 2		2×32
Global Attention Pool		128
Dense		$4N$
Parameters		Values
Activation		ReLU
Optimizer		Adam
Loss		MSE
Learning Rate		$1e-3$
L_2 Regularization		$5e-4$

\mathbf{A} denotes that a single edge connects two nodes as depicted in Fig. 4. It is worth noting that this crucial and unconventional approach enables to track the phase changes during the pilot signaling and reveal the channel characteristics. Also, the dataset includes the weight matrix of the edge for the j -th non-zero element of the adjacency matrix given as

$$\mathbf{E}_j = \mathbf{s}, \mathbf{E} \in \mathbb{C}^{2 \times 2 \times M}. \quad (12)$$

The label vector, \mathbf{y} , including the known channel coefficients is generated as

$$\mathbf{y} = [h_1, h_2, \dots, h_N, g_1, g_2, \dots, g_N]^T. \quad (13)$$

The training dataset consists of 1000 input samples for each SNR level within -30 dB and 0 dB. The step size for SNR levels is 2 dB. The total number of input samples in the training dataset is 16000 for each N , and SNR values. The training dataset has been divided into two parts: training and validation with the rate of 4 : 1. Table I summarizes the parameters that are used during the dataset generation.

B. GAT Model and Training

This section details the parameters of the proposed GAT model that is implemented by using Spektral [45]. The model consists of two consecutive GALs. The first and second

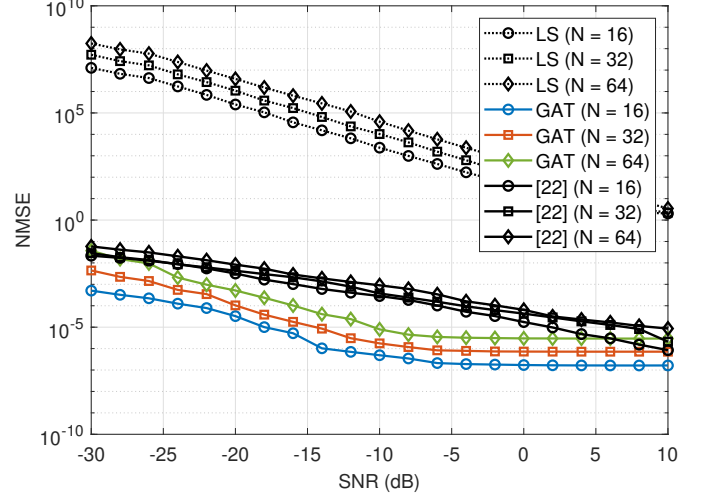


Fig. 5. NMSE performance of the proposed GAT-aided RIS-assisted satellite-to-IoT cascaded channel estimation versus the SNRs, the number of RIS elements, N for $M_p = 16$ and $K = 10$. It should be noted that $M_p = 256$ for [22].

layers have 128 and 32 output channels, respectively. Each layer employs the ReLU activation function. The size of the input becomes $P = 2$, $F = M$, and $S = M$. Following GALs, a global attention pooling layer is utilized to avoid the model overfitting by decreasing the number of representations. Moreover, it is worth noting that each GAL dropouts fifty percent of the representations in order to reduce the model complexity as well avoiding overfitting.

Besides dropouts, the network employs L_2 regularization. The learning flow through the network is terminated by a hidden layer with $4N$ neurons. In accordance with the nature of the channel estimation problem, the loss function is chosen as mean square error (MSE). To minimize the loss function, ADAM optimizer with a learning rate of 10^{-3} is employed when compiling the network. Although the number of epochs is determined as 20, the early stopping is activated to keep training time short if the loss function does not decrease for 5 epochs. Table II summarizes the GAT parameters and inputs.

V. NUMERICAL RESULTS AND DISCUSSIONS

In this section, the performance of RIS-assisted satellite IoT communications is investigated under GAT channel estimation procedure detailed in the previous section. As [24] denotes

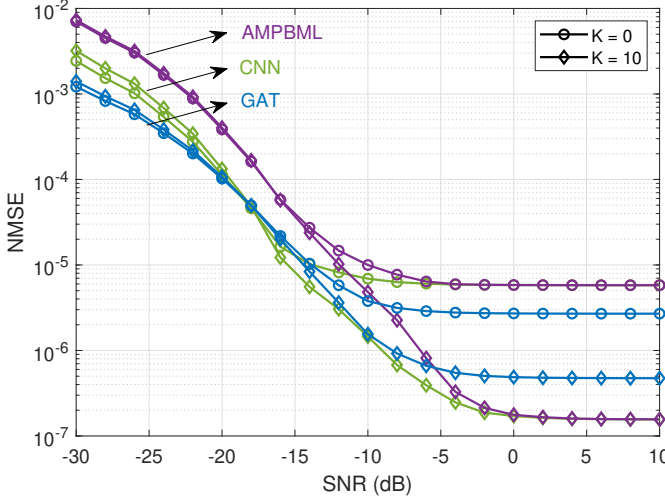


Fig. 6. NMSE performance of the proposed GAT and other DL methods, the number of RIS elements, $N = 16$ for $M_p = 16$ and $K = 0$ and 10 . It is observed that the proposed GAT shows a higher performance than the conventional DL methods under changing channel conditions. These results emphasize the importance of attention mechanisms and inductive learning.

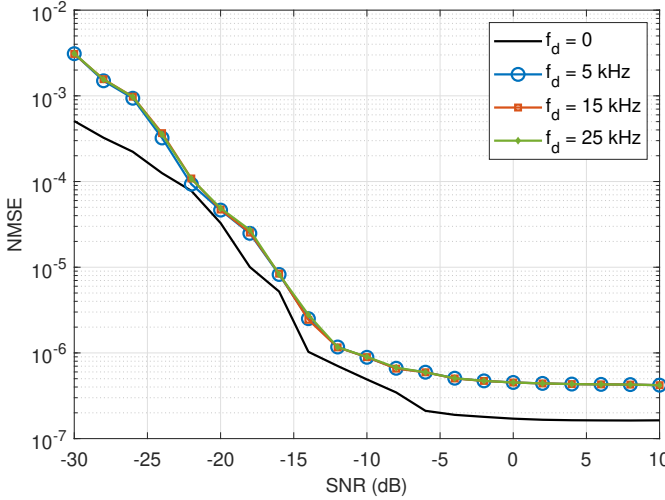


Fig. 7. NMSE performance of the proposed GAT under Doppler shift which observed in LEO satellite communication systems due to motion of satellites. The residual Doppler shift after compensation is denoted by f_d . It is observed that the proposed GAT-based channel estimator can almost maintain the performance under the Doppler shift although the training set does not consist of any Doppler effects. These results also denote the importance of attention mechanisms and inductive learning.

that the GAT estimator is able to keep the same estimation performance for the decreasing number of pilot symbols. Therefore, we keep the length of pilot signaling as much as possible to avoid pilot contamination. In this study, the number of pilot symbols, M_p is selected as 16. Moreover, the GAT estimator is robust to changes in fading statistics, due to attention mechanism [24, 25]. In this study, we consider only Rician fading with the shape parameter of $K = 10$ to allow slight non-line-of-sight (NLOS) components in the channel model as given in [31–33]. The simulation parameters are summarized in the test column of Table I.

Firstly, the channel estimation performances for both \mathbf{h} and

\mathbf{g} are considered in Fig. 5. The proposed GAT estimator outperforms LS estimation in terms of NMSE. It is seen that both methods require an additional 3 dB SNR when the number of meta-atoms is doubled. But, it should be noted that the required transmit power reduces 3 dB since doubling the number of elements decreases the required transmit power by 6 dB [12, 13]. However, the proposed GAT estimator is overperformed compared to LS estimator. Furthermore, even though the training set does not include SNR values between 0 and 10 dB, the NMSE performance does not deteriorate as seen in Fig. 5. The NMSE of GAT converges to 10^{-7} for increasing SNR value. Moreover, Fig. 5 denotes that the proposed method can show higher performance compared to [22] while the proposed method uses a one-sixteenth long pilot subframe of [22].

Besides non-DL methods, we evaluate conventional DL methods for the same problem. In this study, we discuss the results of two of the recently proposed conventional DL methods, which have the highest performance, compared with the GAT. AMPBML has been proposed in [46] for beam alignment in mmWave massive MIMO. Another method based on convolutional neural network (CNN) has been proposed in [19] for channel estimation in RIS-assisted mmWave communications. The performance of the models, which have been trained in the case of $K = 10$, is investigated under more challenging conditions by also considering the Rayleigh channel (i.e., $K = 0$) in the test dataset. In Fig. 6, it is shown that the proposed GAT overperforms compared to the conventional methods at low SNR. Although GAT performs slightly lower than conventional methods at high SNR, it maintains its performance much better than the conventional DL methods in changing channel conditions. Owing to the GATs' inductive learning ability over unobserved cases, GAT outperforms the aforementioned machine learning methods when the test data contains different channel conditions than the training dataset. These results reveal how important the attention mechanism is in the cases unobserved during training. Further, more detailed studies are needed on how the conventional methods perform under changing conditions due to a lack of inductive learning capability. As stated above, inductive learning due to the attention mechanism in GATs can allow the network to generalize over unobserved graphs which can mean unobserved channel conditions in this study. It is worth noting that training complexity is another important factor besides performance in DL methods. From this point of view, it is an important advantage to train the proposed GAT model in a shorter time compared to other models. For example, AMPBML and CNN each require 1.8 and 3 times the epoch duration of GAT, respectively. In brief, the proposed GAT both shows a higher performance with increased robustness under changing conditions and has less computational complexity.

Another crucial point in LEO-satellite communications systems that differs from terrestrial point-to-point communication systems is the Doppler effect because of the high mobility of satellites. Therefore, it should be carefully investigated in channel estimation performance since the Doppler shift changes through its orbit (i.e., elevation angle) [47]. From

the point of channel estimation in LEO satellite systems, employing separate models for each Doppler shift or elevation angle is not practical and feasible for channel estimation; hence, the model must be attainable under changing conditions that have not been observed during the training process. We discuss and denote that the proposed method can maintain the performance under changing conditions such as small-scale fading and SNR above. Similar to what changes in small-scale fading affect the received signal phase, the Doppler shift can accumulate phase error on the received signal. Intuitively, it might be said that the proposed method can maintain the performance under the Doppler effect by considering the previous results. Besides the results discussed previously, we investigate the performance of the GAT-based estimator under the Doppler shift.

As given in [47], the maximum Doppler shift for LEO satellite at 600 km altitude is ranging in between -50 and 50 kHz. It should be noted that the higher the maximum Doppler shift is observed, the higher the altitude. Also, as the Doppler shift is monotonic and predictable, it is possible to compensate Doppler shift observed in LEO satellite communications [48]. For example, in [49], maximum a posterior estimator was proposed to exploit the Doppler shift in LEO satellite communication systems. However, residual Doppler shift after compensation can affect the performance of the system and it should be investigated.

First, we generate a test dataset including signal samples that observed the Doppler effect with residual Doppler shifts, f_d , of 5, 15, and 25 kHz after Doppler compensation [49]. Then, the model trained with data without any Doppler impact is tested with the new dataset. The results are shown in Fig. 7 compared to the case without the Doppler shift (i.e., $f_d = 0$). As seen in Fig. 7, the impact of the Doppler shift on the channel estimation performance is very limited likewise the results in Fig. 6. The magnitude of Doppler shifts has no remarkable impact on the performance. The results exhibit generalizability, which is the most desired feature for DL applications under changing conditions, of the proposed method.

Next, the error rate performance of the proposed RIS-assisted DTS IoT system is investigated by considering the channel estimation error resulting from GAT estimator. The channel estimation and then BER analysis are performed for the number of RIS elements of 16, 32, 64. In this case, the RIS is assumed as a continuous phase. The simulation results under both the perfect estimation and GAT estimation are given in Fig. 8. It is observed that BER performance in the case of GAT estimator is almost same as the perfect estimation at the low SNR region. As the SNR value increases, there is a very slight degradation in the error performance due to the non-perfect estimation of the GAT. Moreover, Fig. 9 denotes the confidence intervals for trained GAT estimators. In each training phase, the model parameters and training data are kept the same. However, random initialization and randomness in the optimizer give rise to different trained models with distinct weight matrices. Intuitively, the best case is the almost same as the BER results in the case of the perfect estimation. But, the increasing number of RIS elements makes the confidence interval larger by resulting in the worst channel estimation

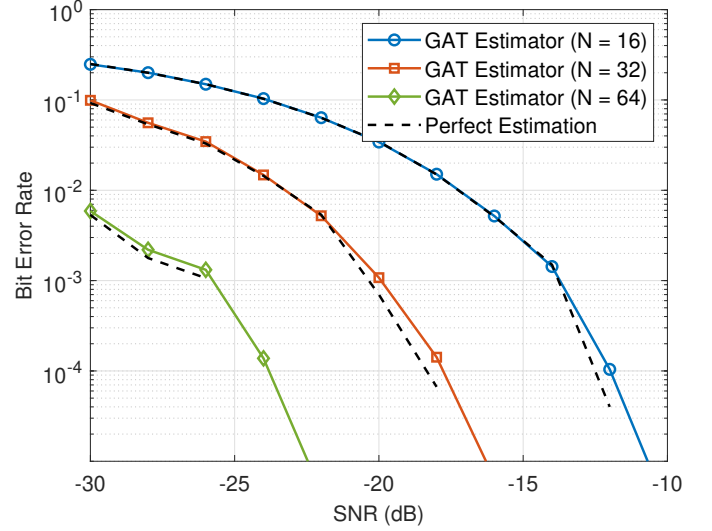


Fig. 8. BER performance of RIS-assisted satellite IoT communications with BPSK signaling under the ideal channel estimation and GAT-based estimation.

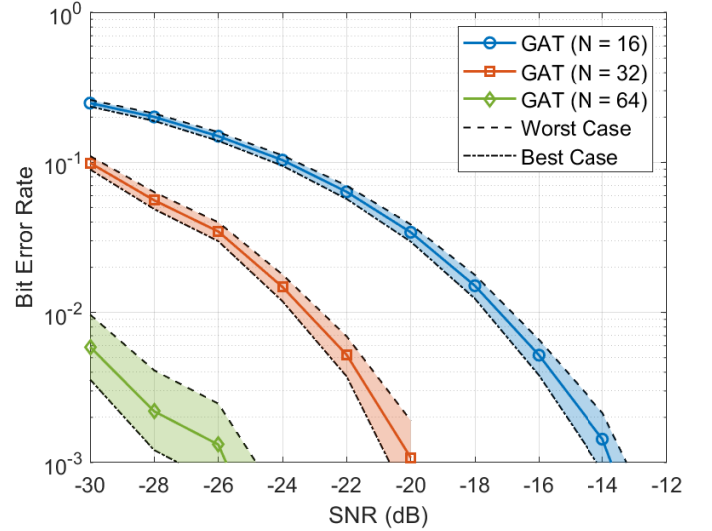


Fig. 9. The confidence interval of BER performance for training procedures. The GATs are trained without any change in the parameters and training sets.

error.

Although RISs can be theoretically considered as continuous phase systems, this assumption is not practically feasible due to hardware limitations. Therefore, we consider discrete-phase RISs with GAT channel estimation. Error rate performance is investigated up to quantized 3-bits RISs with the variable number of elements. First, we assume a basic RIS design which enable phase shifts, ϕ_n , in $[-\pi, \pi)$. The step size in phase shift set supported by RIS is determined by the number of quantization levels as $\frac{2\pi}{2^{N_{\text{bit}}}}$, where N_{bit} stands for the number of bits. It can be heuristically said that the system performance improves if the number of distinct discrete phase shifts that RIS can provide increases, or in other words, converges to the continuous phase case. Fig. 10 gives the BER results for the quantization levels of 2, 4, and 8. The simulation results denote that increase in the number of quantization levels for phase shifts reduces the error probability. As seen

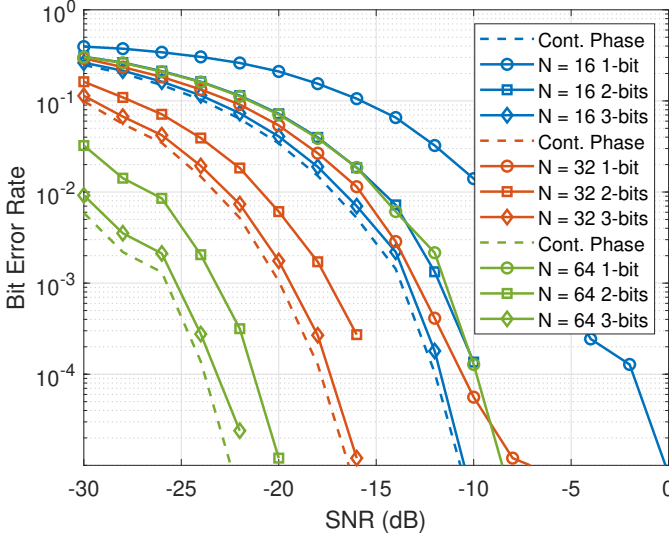


Fig. 10. BER performance of discrete phase RIS-assisted satellite IoT communications with BPSK signaling. Increasing the number of quantization levels proportionally improves the error rate performance of the system.

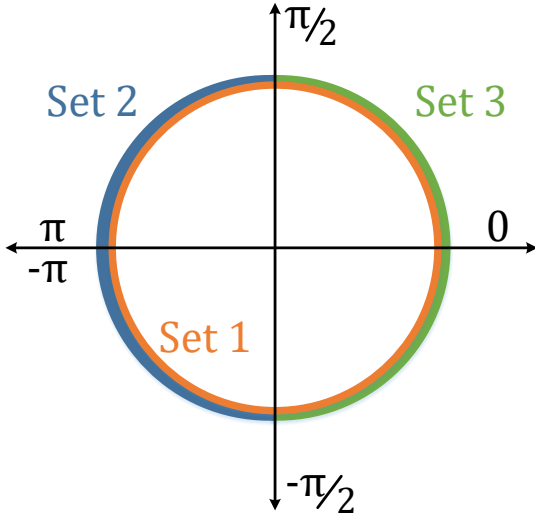


Fig. 11. The illustration for the phase sets on the unit circle.

in Fig. 10, 3-bit RIS designs almost approach the error probabilities that the optimum design can achieve. 1-bit designs can only show the same BER performance at higher SNR values compared to 2-bit designs. In other words, 2-bit designs are much more energy-efficient. In addition, considering the cost of RISs that supports more than 3-bit quantization levels, it is considered feasible to use 3-bit designs for energy-efficient satellite IoT communication systems.

The phase shifts might not be uniformly distributed in $[-\pi, \pi)$ because of the limitations in intelligent metasurface designs. For example, the phase shift span is proportional to the square-root of the ratio between the effective capacitance and the effective inductance [50]. Because the varactor diode reaches the saturation level (i.e., constant capacitance value) although the control voltage increases, all phase shift values

TABLE III
THE PHASE SETS WITH DIFFERENT SPANS BETWEEN $-\pi$ AND π .

Phase Set	Phase Interval	Step Size
Set 1	$[-\pi, \pi)$	$\frac{2\pi}{2^{N_{bit}}}$
Set 2	$(-\pi, -\frac{\pi}{2}] \cup [\frac{\pi}{2}, \pi)$	$\frac{2\pi}{2^{N_{bit}}}$
Set 3	$[-\frac{\pi}{2}, \frac{\pi}{2}]$	$\frac{2\pi}{2^{N_{bit}}}$

may not be supported by the intelligent surface. For instance, the surface in [51] is able to shift the phase of an incident wave by up to 250 degrees. Hence, we investigate the error rate performance versus the different phase shift sets, namely different RIS designs. We evaluate three sets: Set 1 has been already introduced above. Set 2 and Set 3 only consist of the left-hand side and right-hand side of the phase circle, respectively. The phase shift sets are summarized in Table III and illustrated in Fig. 11. Besides, the discrete phase shifts are employed in this analysis. The phase shift, ϕ_n , is determined as the closest phase value in the set to the phase of the channel coefficient estimated by GAT as follows:

$$\phi_n = S\{\phi_k : k = \underset{s}{\operatorname{argmin}}(|\phi_s - \angle(\hat{h}_n \hat{g}_n)|)\}, s = 1, \dots, 2^{N_{bit}}, \quad (14)$$

where S is the phase shift set including discrete phase shifts, ϕ_s . $\angle(\cdot)$ stands for the angle operator. Additionally, h_n and g_n denote the estimated channel coefficients regarding the n -th elements of RIS. Fig. 12 shows the BER performance of RIS-assisted satellite IoT system for the different phase shift sets with 2- and 3-bits. Set 1 and Set 2 show almost similar BER; however, Set 1 results in slightly better error performance. Moreover, BER performance improves when the quantization level increases in the first two sets while increasing the number of bits in Set 3 surprisingly worsens the performance. To explain this, it is necessary to look closely at the channel model. Fig. 13 shows the phase histogram of the actual cascaded channel and the phase histogram of the estimated channel coefficients, respectively. As seen, the phase of the cascaded channel is concentrated around $-\pi$ and π . Likewise, since the channel estimation performance is high, the information about the estimated channels is parallel to the actual channel. These histograms show why Set 1 and Set 2 both performed similarly and have higher performance compared to Set 3. Since the working principle of RIS is to make the SNR maximum by eliminating the phase information of the cascaded channel, RIS must support phase shifts in a way that eliminates the phases of the cascaded channel. Set 1 and Set 2 support the phase shifts of the channels to omit the phases concentrated around $-\pi$ and π . However, since Set 3 consists of phase shifts between $-\pi/2$ and $\pi/2$, it cannot completely exclude actual phases around $\mp\pi$. In addition, increasing the quantization level also allows correcting the actual phases different from $\mp\pi$ in Set 1 and Set 2. The increase in the number of levels enables the generation of new phase values between $-\pi/2$ and $\pi/2$ in Set 3 and creates phase shifts farther away from $\mp\pi$. Therefore, the phase information cannot be adequately corrected.

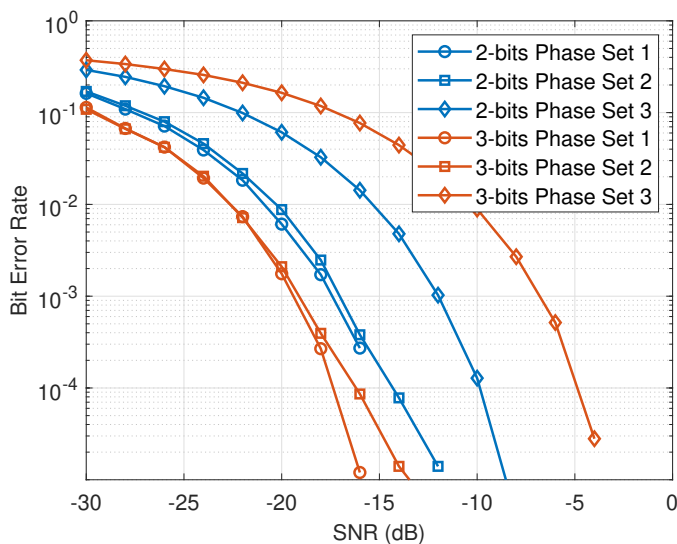


Fig. 12. BER performance of discrete phase 32-elements RIS-assisted satellite IoT communications regarding different phase sets.

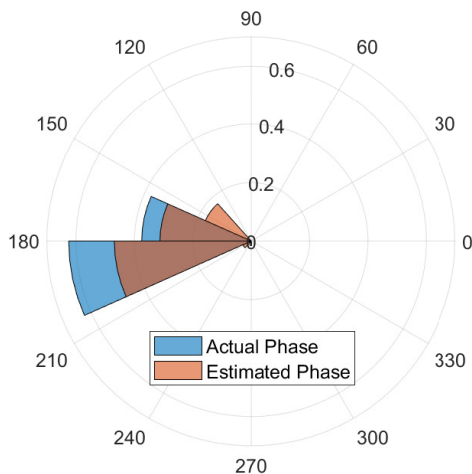


Fig. 13. The histogram for the phase of actual and estimated channel coefficients.

VI. RESEARCH DIRECTIONS AND CONCLUDING REMARKS

In this study, GAT based channel estimation is presented for RIS-assisted communications and it is shown that high performance is achieved. The proposed channel estimation method based on GAT is able to learn inductively; therefore, it can provide high performance under changing conditions that are not included in the training phase.

To improve DtS IoT systems, RIS with GAT is integrated to the system architecture. By doing so, it is demonstrated that the error probability is achieved at lower SNR compared to conventional methods. BER performance under various RIS configurations including discrete and piecewise phase sets is numerically investigated. It is shown that 2-bit resolution can almost perform as well as ideal RISs with a continuous phase shift. In addition, the simulation results show that the channel model is an important design parameter for RISs. This study provides a comprehensive investigation of GAT-

based channel estimation and performance analysis on RIS-assisted DtSs; however, the impact of Doppler shift to GAT performance due to the motion of LEO satellites requires more investigation. It is shown in this study that the proposed GAT-based estimator performs better with much shorter pilot signals compared to the state-of-art methods in the literature. It should be noted that although very low pilot overhead is required with the proposed method, there may be performance losses in estimating the instantaneous CSI due to the movement of LEO satellites. Therefore, in future studies, it is planned to work on performance improvement with the use of average CSI based on the method given in this study. Moreover, RIS fabrication and deployment on satellites requires consideration of space conditions and SWaP constraints, so it should be the subject of interdisciplinary research. Another important point is investigating system performance for the downlink signaling since this study covers only performance analysis for uplink. Due to partial channel reciprocity, it is possible to observe some changes in channel characteristics between uplink and downlink. However, as shown in this study, the GAT-based estimator can provide generalizable results and an adjustment factor can be used with respect to satellite elevation angle to estimate the changes in the downlink channel compared to the uplink channel estimated by the GAT. Furthermore, as impairments in RIS design can seriously affect performance, future studies should consider impairments. For instance, as this study considers all-passive element RIS, the saturation effect is not taken into account. However, the saturation effect must be considered for RIS designs including active elements.

Last but not least, even though this study mainly addresses DtS IoT communication, cooperation between RISs and aggregator gateways which are mainly used in the state-of-the-art satellite IoT applications should be investigated in future studies.

REFERENCES

- [1] A. Nassar and Y. Yilmaz, "Deep reinforcement learning for adaptive network slicing in 5G for intelligent vehicular systems and smart cities," *IEEE Internet Things J.*, vol. 9, no. 1, pp. 222–235, 2022.
- [2] T. Sanislav, G. D. Mois, S. Zeadally, and S. C. Folea, "Energy harvesting techniques for internet of things (IoT)," *IEEE Access*, vol. 9, pp. 39 530–39 549, 2021.
- [3] G. A. Akpakwu, B. J. Silva, G. P. Hancke, and A. M. Abu-Mahfouz, "A survey on 5G networks for the Internet of Things: Communication technologies and challenges," *IEEE Access*, vol. 6, pp. 3619–3647, 2017.
- [4] J. A. Fraire, S. Céspedes, and N. Accettura, "Direct-to-satellite IoT: a survey of the state of the art and future research perspectives," in *International Conference on Ad-Hoc Networks and Wireless*. Springer, 2019, pp. 241–258.
- [5] J. A. Fraire, S. Henn, F. Dovis, R. Garello, and G. Taricco, "Sparse satellite constellation design for LoRa-based direct-to-satellite internet of things," in *IEEE Global Communications Conference*, 2020, pp. 1–6.
- [6] R. Barbau, V. Deslandes, G. Jakllari, J. Tronc, J.-F. Chouteau, and A.-L. Beylot, "NB-IoT over GEO satellite: performance analysis," in *Advanced Satellite Multimedia Systems Conference and the Signal Processing for Space Communications Workshop*, 2020, pp. 1–8.
- [7] C. A. Hofmann and A. Knopp, "Direct access to GEO satellites: An Internet of Remote Things technology," in *IEEE 5G World Forum*, 2019, pp. 578–583.
- [8] S. Cluzel, L. Franck, J. Radzik, S. Cazalens, M. Dervin, C. Baudoin, and D. Dragomirescu, "3GPP NB-IoT coverage extension using LEO satellites," in *IEEE Vehicular Technology Conference*, 2018, pp. 1–5.
- [9] Z. Qu, G. Zhang, H. Cao, and J. Xie, "LEO satellite constellation for Internet of Things," *IEEE Access*, vol. 5, pp. 18 391–18 401, 2017.

- [10] E. Basar, M. Di Renzo, J. De Rosny, M. Debbah, M.-S. Alouini, and R. Zhang, "Wireless communications through reconfigurable intelligent surfaces," *IEEE Access*, vol. 7, pp. 116 753–116 773, 2019.
- [11] Q. Wu and R. Zhang, "Towards smart and reconfigurable environment: Intelligent reflecting surface aided wireless network," *IEEE Commun. Mag.*, vol. 58, no. 1, pp. 106–112, 2019.
- [12] K. Tekbıyık, G. K. Kurt, A. R. Ekti, and H. Yanikomeroglu, "Reconfigurable intelligent surfaces in action for non-terrestrial networks," *IEEE Veh. Technol. Mag.*, vol. *Early Access*, pp. 1–10, 2022.
- [13] —, "Reconfigurable intelligent surface empowered terahertz communication for LEO satellite networks," *arXiv preprint arXiv:2007.04281*, 2020.
- [14] L. Dai, B. Wang, M. Wang, X. Yang, J. Tan, S. Bi, S. Xu, F. Yang, Z. Chen, M. Di Renzo *et al.*, "Reconfigurable intelligent surface-based wireless communications: Antenna design, prototyping, and experimental results," *IEEE Access*, vol. 8, pp. 45 913–45 923, 2020.
- [15] W. Tang, J. Y. Dai, M. Z. Chen, K.-K. Wong, X. Li, X. Zhao, S. Jin, Q. Cheng, and T. J. Cui, "MIMO transmission through reconfigurable intelligent surface: System design, analysis, and implementation," *IEEE J. Sel. Areas Commun.*, vol. 38, no. 11, pp. 2683–2699, 2020.
- [16] J. Hu, H. Zhang, B. Di, L. Li, K. Bian, L. Song, Y. Li, Z. Han, and H. V. Poor, "Reconfigurable intelligent surface based RF sensing: Design, optimization, and implementation," *IEEE J. Sel. Areas Commun.*, vol. 38, no. 11, pp. 2700–2716, 2020.
- [17] C. Huang, A. Zappone, G. C. Alexandropoulos, M. Debbah, and C. Yuen, "Reconfigurable intelligent surfaces for energy efficiency in wireless communication," *IEEE Trans. on Wirel. Commun.*, vol. 18, no. 8, pp. 4157–4170, 2019.
- [18] K. Tekbıyık, G. K. Kurt, and H. Yanikomeroglu, "Energy-efficient RIS-assisted satellites for IoT networks," *IEEE Internet Things J. Early Access*, pp. 1–10, 2021.
- [19] A. M. Elbir, A. Papazafeiropoulos, P. Kourtessis, and S. Chatzinotas, "Deep channel learning for large intelligent surfaces aided mm-Wave massive MIMO systems," *IEEE Wireless Commun. Lett.*, vol. 9, no. 9, pp. 1447–1451, 2020.
- [20] D. Mishra and H. Johansson, "Channel estimation and low-complexity beamforming design for passive intelligent surface assisted MISO wireless energy transfer," in *Proc. IEEE ICASSP*, 2019, pp. 4659–4663.
- [21] G. E. Corazza and F. Vatalaro, "A statistical model for land mobile satellite channels and its application to nongeostationary orbit systems," *IEEE Trans. Veh. Technol.*, vol. 43, no. 3, pp. 738–742, 1994.
- [22] J. Chen, Y.-C. Liang, H. V. Cheng, and W. Yu, "Channel estimation for reconfigurable intelligent surface aided multi-user MIMO systems," *arXiv preprint arXiv:1912.03619*, 2019.
- [23] A. Taha, M. Alrabeiah, and A. Alkhatieb, "Enabling large intelligent surfaces with compressive sensing and deep learning," *IEEE Access*, vol. 9, pp. 44 304–44 321, 2021.
- [24] K. Tekbıyık, G. K. Kurt, C. Huang, A. R. Ekti, and H. Yanikomeroglu, "Channel estimation for full-duplex RIS-assisted HAPS backhauling with graph attention networks," in *IEEE International Conference on Communications*, 2021, pp. 1–6.
- [25] P. Veličković, G. Cucurull, A. Casanova, A. Romero, P. Lio, and Y. Bengio, "Graph attention networks," in *The International Conference on Learning Representations*, 2018, pp. 1–12.
- [26] J. Lee, I. Lee, and J. Kang, "Self-attention graph pooling," in *Proceedings of the 36th International Conference on Machine Learning*, vol. 97. PMLR, 09–15 Jun 2019, pp. 3734–3743.
- [27] E. Basar, "Reconfigurable intelligent surfaces for Doppler effect and multipath fading mitigation," *Frontiers in Communications and Networks*, p. 14, 2021.
- [28] I. Yildirim, A. Uyrus, and E. Basar, "Modeling and analysis of reconfigurable intelligent surfaces for indoor and outdoor applications in future wireless networks," *IEEE Trans. on Commun.*, vol. 69, no. 2, pp. 1290–1301, 2021.
- [29] D. Bahdanau, K. Cho, and Y. Bengio, "Neural machine translation by jointly learning to align and translate," *arXiv preprint arXiv:1409.0473*, 2014.
- [30] W. Tang, M. Z. Chen, X. Chen, J. Y. Dai, Y. Han, M. Di Renzo, Y. Zeng, S. Jin, Q. Cheng, and T. J. Cui, "Wireless communications with reconfigurable intelligent surface: Path loss modeling and experimental measurement," *IEEE Transactions on Wireless Communications*, vol. 20, no. 1, pp. 421–439, 2020.
- [31] N. Letzepis and A. J. Grant, "Capacity of the multiple spot beam satellite channel with Rician fading," *IEEE Trans. Inf. Theory*, vol. 54, no. 11, pp. 5210–5222, 2008.
- [32] L. You, K.-X. Li, J. Wang, X. Gao, X.-G. Xia, and B. Ottersten, "Massive MIMO transmission for LEO satellite communications," *IEEE J. Sel. Areas Commun.*, vol. 38, no. 8, pp. 1851–1865, 2020.
- [33] D.-H. Jung, J.-G. Ryu, W.-J. Byun, and J. Choi, "Performance analysis of satellite communication system under the shadowed-rician fading: A stochastic geometry approach," *IEEE Transactions on Communications*, vol. 70, no. 4, pp. 2707–2721, 2022.
- [34] M. Anteur, V. Deslandes, N. Thomas, and A.-L. Beylot, "Ultra narrow band technique for low power wide area communications," in *IEEE Global Communications Conference*, 2015, pp. 1–6.
- [35] T. Lassen, "Long-range RF communication: Why narrowband is the de facto standard," <https://www.ti.com/lit/wp/swry006/swry006.pdf>, 2014, (Accessed on 14/12/2021).
- [36] X. Xiong, K. Zheng, R. Xu, W. Xiang, and P. Chatzimisios, "Low power wide area machine-to-machine networks: key techniques and prototype," *IEEE Commun. Mag.*, vol. 53, no. 9, pp. 64–71, 2015.
- [37] F. Panchaldi, G. M. Vitetta, R. Kalbasi, N. Al-Dhahir, M. Uysal, and H. Mheidat, "Single-carrier frequency domain equalization," *IEEE Signal Processing Magazine*, vol. 25, no. 5, pp. 37–56, 2008.
- [38] N. Benvenuto, R. Dinis, D. Falconer, and S. Tomasin, "Single carrier modulation with nonlinear frequency domain equalization: An idea whose time has come—Again," *Proceedings of the IEEE*, vol. 98, no. 1, pp. 69–96, 2009.
- [39] L. Zhang, A. Ijaz, P. Xiao, and R. Tafazolli, "Channel equalization and interference analysis for uplink narrowband Internet of Things (NB-IoT)," *IEEE Communications Letters*, vol. 21, no. 10, pp. 2206–2209, 2017.
- [40] S. Popli, R. K. Jha, and S. Jain, "A survey on energy efficient narrowband internet of things (NB-IoT): Architecture, application and challenges," *IEEE Access*, vol. 7, pp. 16 739–16 776, 2018.
- [41] M. S. Ali, M. K. H. Jewel, Y. Li, and F. Lin, "Frequency-domain channel equalisation for LTE-based uplink narrowband Internet of Things systems," *IET Communications*, vol. 13, no. 3, pp. 281–288, 2019.
- [42] E. Arslan, I. Yildirim, F. Kilinc, and E. Basar, "Over-the-air equalization with reconfigurable intelligent surfaces," *arXiv preprint arXiv:2106.07996*, 2021.
- [43] C. A. Hofmann and A. Knopp, "Ultranarrowband waveform for IoT direct random multiple access to GEO satellites," *IEEE Internet Things J.*, vol. 6, no. 6, pp. 10 134–10 149, 2019.
- [44] P. Kim, S. Jung, D.-h. Jung, J.-G. Ryu, and D.-G. Oh, "Performance analysis of direct sequence spread spectrum ALOHA for LEO satellite based IoT service," in *IEEE 90th Vehicular Technology Conference (VTC2019-Fall)*, 2019, pp. 1–5.
- [45] D. Grattarola and C. Alippi, "Graph neural networks in Tensorflow and Keras with Spektral," *IEEE Comput. Intell. Mag.*, vol. 16, no. 1, pp. 99–106.
- [46] W. Ma, C. Qi, and G. Y. Li, "Machine learning for beam alignment in millimeter wave massive MIMO," *IEEE Wireless Commun. Lett.*, vol. 9, no. 6, pp. 875–878, 2020.
- [47] T. K. Nguyen, C. T. Nguyen, H. D. Le, and A. T. Pham, "TCP performance over satellite-based hybrid FSO/RF vehicular networks: Modeling and analysis," *IEEE Access*, vol. 9, pp. 108 426–108 440, 2021.
- [48] O. Kodheli, N. Maturo, S. Chatzinotas, S. Andrenacci, and F. Zimmer, "On the random access procedure of NB-IoT non-terrestrial networks," in *2020 10th Advanced Satellite Multimedia Systems Conference and the 16th Signal Processing for Space Communications Workshop (ASMS/SPSC)*, 2020, pp. 1–8.
- [49] J. Lin, Z. Hou, Y. Zhou, L. Tian, and J. Shi, "MAP estimation based on Doppler characterization in broadband and mobile LEO satellite communications," in *IEEE 83rd Vehicular Technology Conference (VTC Spring)*, 2016, pp. 1–5.
- [50] F. Liu, O. Tsilipakos, A. Pitolakis, A. C. Tzamalidou, M. S. Mirmoosa, N. V. Kantartzis, D.-H. Kwon, J. Georgiou, K. Kossifos, M. A. Antoniadis *et al.*, "Intelligent metasurfaces with continuously tunable local surface impedance for multiple reconfigurable functions," *Physical Review Applied*, vol. 11, no. 4, p. 044024, 2019.
- [51] W. Tang, X. Li, J. Y. Dai, S. Jin, Y. Zeng, Q. Cheng, and T. J. Cui, "Wireless communications with programmable metasurface: Transceiver design and experimental results," *China Communications*, vol. 16, no. 5, pp. 46–61, 2019.